Heliyon 10 (2024) e32864

Contents lists available at ScienceDirect

Heliyon

journal homepage: www.cell.com/heliyon

Research article

Fabrication of pH-stimuli hydrogel as bioactive materials for wound healing applications

Liang Cheng , Song Zhang , Qian Zhang , Wenjie Gao , Benfeng Wang , Shengzhi Mu *

Department of Burns and Plastic Surgery, Shaanxi Provincial People's Hospital, Xi'an, 710068, China

ARTICLE INFO

Keywords:
Carboxymethyl cellulose
Polyvinyl alcohol
Gelatin
Drug delivery
Tissue engineering
Wound healing

ABSTRACT

Hydrogels exhibit exceptional suitability as wound dressing due to their remarkable three-dimensional (3D) characteristics. Here, we have reported the fabrication of hydrogels from biopolymers carboxymethyl cellulose (CMC), polyvinyl alcohol (PVA), and gelatin via a simple blending method to mimic the natural extracellular matrix. Scanning electron microscopy (SEM), water contact meters (WCM), and Fourier-transform infrared spectroscopy (FTIR) were used to evaluate the chemical structural, morphological, and wettability behavior. The wetting and degradation behavior were also found to be different for different formulations (Min. (51.60^{o}) and Max. (113.60^{o})) and (Min. (38.82 mg) and Max. (3.72 mg)), respectively. Swelling was investigated in different media, including phosphate buffer saline solution (PBS) and aqueous media. It was observed that the hydrogel displayed the highest degree of swelling in an aqueous medium (Min. (597.32–1121.49 %) and Max. (1089.51–2139.73 %)) compared to PBS media (Min. (567.01–1021.85 %) and Max. (899.13–1639.17 %)). The release of Neomycin was studied in a PBS medium via the Franz diffusion method at 37 °C. The maximal release in various media demonstrated pH-responsive behavior. The viability and proliferation of fibroblast (3T3) cell lines were examined in vitro to evaluate cytocompatibility. Human Embryonic Kidney (HEK) 293 cells were used to evaluate the hydrogels' ability to promote vascularization and angiogenesis. Therefore, the data demonstrate that hydrogels that have been manufactured have qualities that make them promising for use as wound dressings in wound healing applications.

1. Introduction

The severe wounds, encompassing injuries, acute trauma, and surgical procedures, have progressively escalated, leading to a notable rise in the challenges associated with treating and recovering individuals afflicted with such wounds. The management of these disorders necessitates the utilization of dressings to expedite the wound healing process [1,2]. Inadequately dressed wounds can lead to a protracted healing process and significantly increase the likelihood of infection. Proper wound dressings are crucial for preventing bacterial invasion, mitigating blood outflow, and reducing infection risk [3,4]. Considerable focus has been dedicated to investigating and developing dressing materials utilized in wound healing throughout recent decades. Hydrogels possess various advantageous characteristics that make them highly suitable for utilization as dressing materials in wound management [5,6]. These properties include establishing and sustaining a moist environment, effectively absorbing significant exudate amounts, offering soft-textured moist pads, exhibiting responsiveness to stimuli, and enabling the controlled release of therapeutic agents [7].

* Corresponding author.
E-mail addresses: wbf123789@sina.com (B. Wang), mszping@163.com (S. Mu).

https://doi.org/10.1016/j.heliyon.2024.e32864
Received 5 March 2024; Received in revised form 10 June 2024; Accepted 11 June 2024
Available online 15 June 2024

Specifically, the dynamic movement of the skin can have implications for wound healing, primarily when the wounds are located in areas of the body that are very elastic. If the dressing lacks notable ductility and self-healing properties, it can lead to secondary injury and an extended duration of the healing process [2,8]. Self-repairing hydrogels can retain their effectiveness and structural integrity within intricate physiological surroundings. The utilization of dynamic covalent borate ester linkages to restore hydrogel networks and achieve favorable self-healing qualities has garnered significant interest within the field of hydrogels with self-healing capabilities [9,10]. Natural polymer-based hydrogels demonstrate significant bioactivity and biocompatibility in skin wound healing applications. The potential of these hydrogels to effectively integrate reliable antibacterial properties and biocompatibility while maintaining their physicochemical ability is a topic of significant interest and importance in biomedical applications [11]. An effective approach for enhancing bioactivity, antibacterial, and biodegradability involves the integration of appropriate fillers inside the polymeric matrix [12]. Gelatin has garnered significant interest as a sustainable reinforcing material owing to its biocompatibility derived from natural sources and exceptional biological characteristics [13,14]. The inherent arrangement of gelatin into distinct hierarchical architectures facilitates enhanced interactions between neighboring biological microenvironments, resulting in the concurrent enhancement of physicochemical and biological properties [15,16]. Developing elastic and bioactive hydrogels is crucial for fabricating bio-mimetic skin and fabricating effective wound dressings with improved mechanical properties. Hence, incorporating multifunctional cellulose into gelatin-based hydrogels facilitates the incorporation of desirable properties such as superior ductility, self-adaptability, biodegradability, and biocompatibility [17,18]. PVA is a synthetic polymer with numerous potential physicochemical and biomedical properties and has been extensively used in several biomedical applications [19]. The famous biomedical applications include hard tissue engineering, soft/skin tissue, and wound healing with sustained and controlled drug delivery [20,21]. Carboxymethyl cellulose (CMC) is the modified form of cellulose, a biopolymer with several biomedical applications, including tissue engineering, wound healing, and drug delivery. It has several other potential biomedical characteristics, such as biocompatibility, rheology, hydrophilicity, and biodegradability [22]. Consequently, it is frequently employed in the biomedical sector. Considerable research and development endeavors have been focused on creating hydrogels using metal nanoparticles that are exceptionally well-suited for biomedical purposes [22,23].

Conversely, the process of wound healing is commonly accompanied by bacterial infection. Using antibiotics or integrating bioactive compounds into dressings in therapeutic applications represents a prevalent and productive approach to addressing infections [24]. Neomycin (NEO), an aminoglycoside antibiotic characterized by its high solubility in water and potent antibacterial properties against Gram-positive and Gram-negative bacteria, has been employed in treating bacterial wound infections [25,26]. Hence, integrating NEO into hydrogel structures through dynamic covalent bonding offers a potential solution for achieving prolonged antibiotic release at a wound's site, mitigating the risk of infections over an extended period, and enhancing therapeutic efficacy. It has effectively resulted in the objective of our ongoing research [27].

Based on those explained above, it is of prevailing importance to design a multifunctional and bioactive hydrogel as a wound dressing that acts as a barrier to promote wound healing with improved mechanical stability, reliable moldability, and stretchability. However, achieving the synergistic performances of bioactivity, biocompatibility, and stable mechanical ability, combined with pH-responsive controlled drug release, remains a critical challenge. Here, we develop multifunctional hybrid hydrogels based on a gelatin matrix that interacts with carboxymethyl cellulose, PVA, and graphene oxide (GO) that act as a dual-reinforced network inside the hydrogel. Moreover, CMC could be cross-linked with the Tetraethyl orthosilicate (TEOS) in the polymeric network and oven-dried to get porous hydrogels. Thus, the drug-loaded hydrogel can facilitate local drug delivery under pH-stimuli response to participate actively in wound healing. FTIR and SEM characterized the fabricated hydrogels to evaluate their structural and surface morphological properties. The analysis, such as swelling, wetting, degradation, and water retention, was performed to determine their physicochemical behavior. The cell viability and proliferation assays were performed against fibroblast 3t3 cell lines to determine biocompatibility.

2. Materials and methods

2.1. Materials

Carboxymethyl cellulose (CAS No. C5678-500G) with average molecular weight and medium viscosity (Mw ~90,000 and 50–200 cP), Gelatin from bovine skin (CAS No. G9382-500 g) with 5.10–5.80 mPa s (pH 5.20–5.60), polyvinyl alcohol (CAS No. 341584-500G) with average molecular weight (Mw 89,000–98,000) and density (1.19–1.31 g/cm^3), Tetraethyl orthosilicate (CAS No. 131903-500 ML), Graphene oxide (CAS No. 763713-1G), Neomycin, potassium persulfate (KPS), sodium hydroxide (NaOH), glacial acetic acid, and absolute ethanol were provided by Sigma Aldrich. Fibroblast (3T3) and Human Embryonic Kidney (HEK) 293 cell lines were purchased from the American Type Culture Collection (ATCC). α-MEM, Glutamine penicillin/streptomycin, and Fetal bovine serum (FBS) were bought from Hyclone Laboratories and Thermo Fisher Scientific, respectively. All chemicals were analytically graded and were used without any purification.

2.2. Methods

2.2.1. Graphene oxide functionalized carboxymethyl cellulose

The graphene oxide-*functionalized*-carboxymethyl cellulose (GO-*f*-CMC) was obtained by hydrothermal method using CMC and GO by different GO amounts (0.02, 0.04, and 0.03 mg). Concisely, 3 g of CMC was dispersed into 25 mL deionized water, followed by a variable amount of GO, and stirred at 450 rpm for 3 h to have a homogenized polymeric suspension. Then, it was transferred into

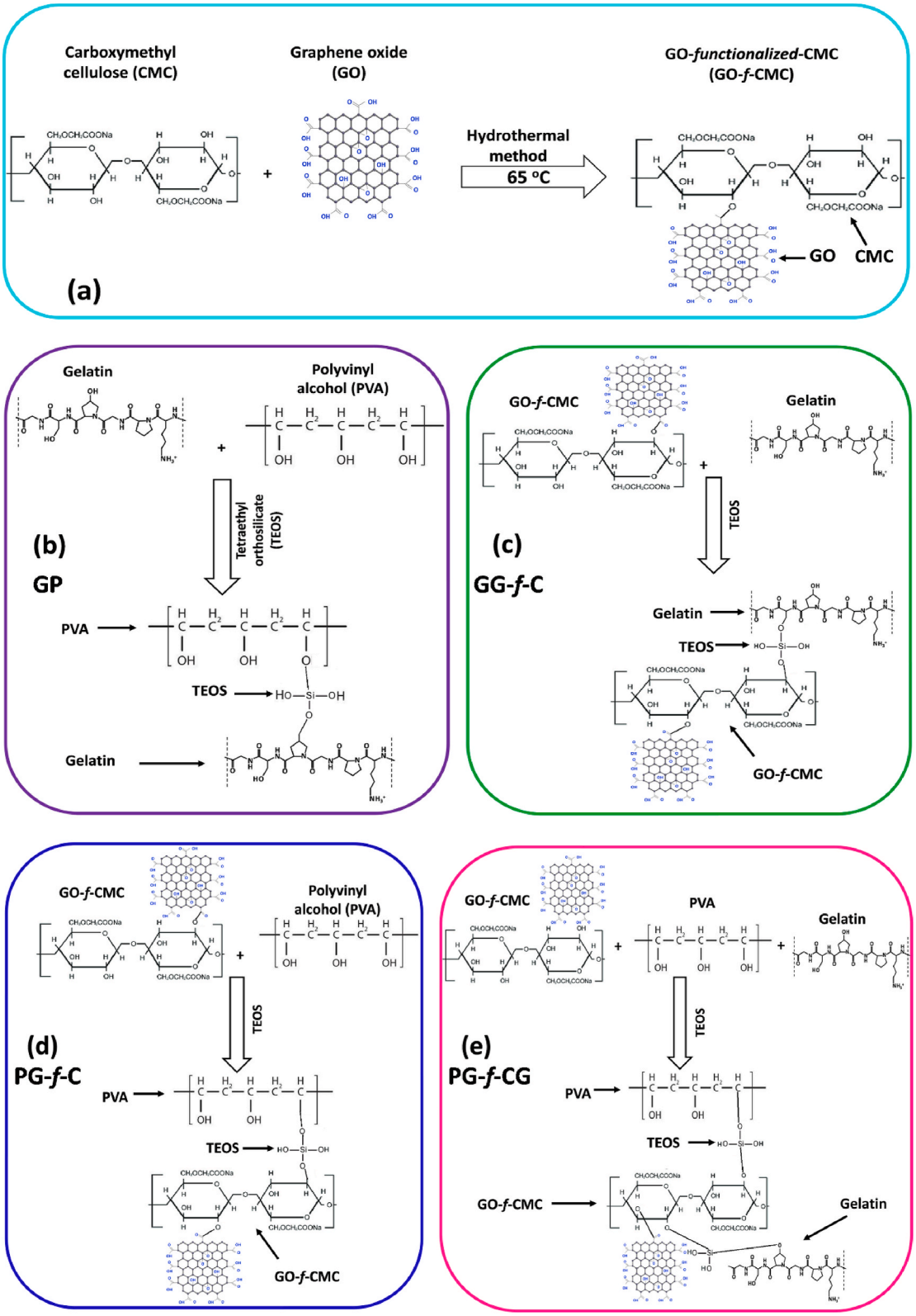

(caption on next page)

Fig. 1. The proposed chemical reaction during the fabrication of hydrogels. (a) graphene oxide-*functionalized*-carboxymethyl cellulose (GO-*f*-CMC) by hydrothermal method. (b) gelatin and polyvinyl alcohol (PVA) and crosslinked with Tetraethyl orthosilicate (TEOS) by a simple blending method. (c) GO-*f*-CMC and gelatin crosslinked with TEOS by simple blending method. (d) GO-*f*-CMC and PVA are crosslinked with TEOS by a simple blending method, and (e) Gelatin, GO-f-CMC, and PVA are crosslinked with TEOS by a simple blending method.

stainless steel separately and put into a heating oven at 60 °C for 12 h to get GO-*f*-CMC (G-*f*-C) polymeric composite mixture. The proposed chemical reaction has been illustrated in Fig. 1.

2.2.2. Fabrication of hydrogels

The synthesized polymeric composite mixture was placed into 25 mL of deionized water and stirred to get the homogenized polymeric blended mixture. Then, 3 g of gelatin was dispersed into 15 mL under constant stirring for 1 h, and PVA polymeric solution was prepared by dissolving 4 g into 10 mL deionized water by heating at 80 °C. Then, different formulations of PVA and gelatin were formulated with the polymeric composite mixture (GO-*f*-CMC), as summarized in Table 1, separately and stirred at 55 °C for 1 h to have a homogenized polymeric mixture. Then, 240 μL of TEOS was dissolved into 5 mL of ethanol and dropwise added to the polymeric mixture's whirlpool, followed by KPS addition to initiate the chemical reaction and stirred at 55 °C for another 3 h. After 3 h, the polymeric mixture was crosslinked to form hydrogels, and 30 mL polymeric solution was poured into Petri dishes. The proposed chemical reaction has been illustrated in Fig. 1(a–e). It was then allowed to cool down at room temperature and placed into an oven at 40 °C for 48 h to get dried hydrogel films. These hydrogel films were peeled off, packed, and stored for further analysis, and the liquid hydrogel was stored in glass vials for biological assays. These hydrogels were coded according to their different formulation and abbreviated in Table 1.

2.3. Neomycin loading

Neomycin is a water-soluble antibiotic drug considered a model drug for investigating release behavior. Therefore, we took 25 mg and dissolved it in 5 mL of deionized water and dropwise to the polymeric suspension of PVA, G-*f*-C, and gelatin. The rest was stirred for 1 h to have a homogenized mixture at 55 °C. Then, 240 μL of Tetraethyl orthosilicate (for crosslinking) was added into 5 mL of absolute ethanol and dropwise into the polymeric mixture, followed by KPS to initiate the crosslinking between the polymeric chain and allowed to stir at 55 °C for 3 h. After 3 h, the successful crosslinking could be developed, Neomycin loaded, and the drug-loaded hydrogel formulations transferred into Patri dishes. These Patri dishes were placed into an oven at 55 °C for 48 h to get well-dried hydrogel films for drug release analysis.

3. Characterizations

The structural behavior and functional group identification of the fabricated hydrogels was conducted by Fourier transform infrared spectroscopy (Shimadzu FTIR-8100A, Japan) in the 4000–600 cm^{-1} range under ATR mode. The surface morphology was studied via a Scanning Electron Microscope (JEOL-JSM 5410 LV) with an accelerated 5 kV voltage. The hydrogel films were dried well and gold-coated before SEM analysis. The atomic force microscopy (Park System XE-100) was employed to determine the surface roughness of the hydrogel. We have used oven-dried hydrogels to evaluate the surface roughness of the hydrogels. Double-sided magnetic tape over the sample stub fixed the hydrogels (1 mm thickness). The hydrophilicity and hydrophobicity of the well-dried hydrogels were investigated by a water contact system (JY-82, Dingsheng, Chengde, China) to determine their wettability.

3.1. Physicochemical analysis

3.1.1. Swelling analysis

The swelling behavior of hydrogel films was evaluated against different media, including deionized water (aqueous) and phosphate buffer saline (PBS) at 37 °C for 24 h in different media pH ranges (pH 1–13). These media with different pH were prepared by appropriate adding acetic acid (CH_3COOH) and sodium hydroxide (NaOH) and their pH was adjusted by a pH-meter. The hydrogels were sliced and weighed accurately at 50 mg as initial weight (Wi) and placed in an already defined medium (aqueous and PBS). The hydrogels were removed after 24 h and their surface water was used by filter paper. The weight of the hydrogels was recorded and was taken as the final weight (W_f), and the swelling of the hydrogels was calculated by Eq. (1).

Table 1
The chemical composition and formulations of different fabricated hydrogels were summarized.

Hydrogel Formulations	Gelatin solution (mL)	PVA solution (mL)	GO-*f*-CMC solution (mL)	TEOS (μL)
GP (**GP**)	10	10	–	240
Gel-GO-*f*-CMC (**GG-*f*-C**)	10	–	10	240
PVA-GO-*f*-CMC (**PG-*f*-C**)	–	10	10	240
PVA-GO-*f*-CMC-Gel (**PG-*f*-CG**)	10	10	10	240

$$\textbf{\textit{Swelling}}\ (\%) = \frac{W_f - W_i}{W_i} \times 100 \quad (1)$$

3.1.2. Degradation analysis

Biomaterial degradation is an essential phenomenon performed in PBS media with pH 7.4 at 37 °C. The hydrogel film was sliced and weighed 50 mg, taken as the initial weight, and placed in the tea bag. The tea bag was placed in PBS media to determine the degradation by desolation behavior after different intervals. After various time intervals, the hydrogel sample was removed from PBS media to remove the tea bag and additional surface media. Then, the weight was measured after a specific time interval (W_t), and degradation behavior was calculated using Eq. (2).

$$\textbf{\textit{Degradation}}\ (\%) = \frac{\boldsymbol{W_i - W_t}}{\boldsymbol{W_i}} \times \mathbf{100} \quad (2)$$

3.2. In vitro assays

3.2.1. Drug delivery

The drug release behavior of the hydrogels was determined using the Franz diffusion method in PBS media. The pH of PBS media was maintained at 7.4, and the temperature was kept at 37 °C. The drug release assay was performed by taking a 2 mL sample from the PBS media and performing its analysis against a double-beam UV–vis spectrophotometer to analyze the released drug concentration in PBS media. The reference was taken as PBS media, and the standard curve was employed to determine the drug-releasing behavior of different formulations.

3.2.2. Cell morphology

Cellular behavior is an important phenomenon, and we have evaluated the cell morphology using the method already reported by Ullah et al. [28]. Briefly, the bottom of 24 well plates was treated with gelatin (0.1 %) as positive control and placed in UV to sterilize for 3 h. Then, the maintained cell lines in α-MEM media were seeded about 5000 cells/cm^2 in the well plate, and hydrogel was placed. These well plates were incubated under standard in vitro conditions (37 °C, with 5 % CO_2 and 90 % humidity). The cell morphology of the fibroblast cell lines was observed after different time intervals (24, 48, and 72 h) by Nikon Eclipse TS100 inverted microscope.

3.2.3. Cell viability and proliferation

The biocompatibility of the fabricated hydrogel was determined by cell viability and proliferation (optical density (O.D.) taken as cell proliferation) against fibroblast (*3T3*) after different time intervals (24, 48, and 72 h) using different hydrogel concentrations (1.5–2.0 μg/mL). The assay was conducted under standard in vitro conditions (pH 7.4, 37 °C, and humidity 90 %). The well plate was coated with gelatin (0.1 %), which was taken as a positive control, and the assay was performed using the Neutral Red method, as reported by Repetto et al. [29]. These cells loaded well plates were treated with Neutral Red (NR) media and incubated for 2 h. After incubation, the excessive NR media was treated with PBS media, and cellular density was investigated with the cell counter. The cell viability was calculated using the following Eq. (3).

$$\textbf{\textit{Cell viability}}\ (\%) = \frac{\boldsymbol{OD_S}}{\boldsymbol{OD_C}} \times \mathbf{100} \quad (3)$$

OD*s* = optical density of the sample, and OD*c* = optical density of control.

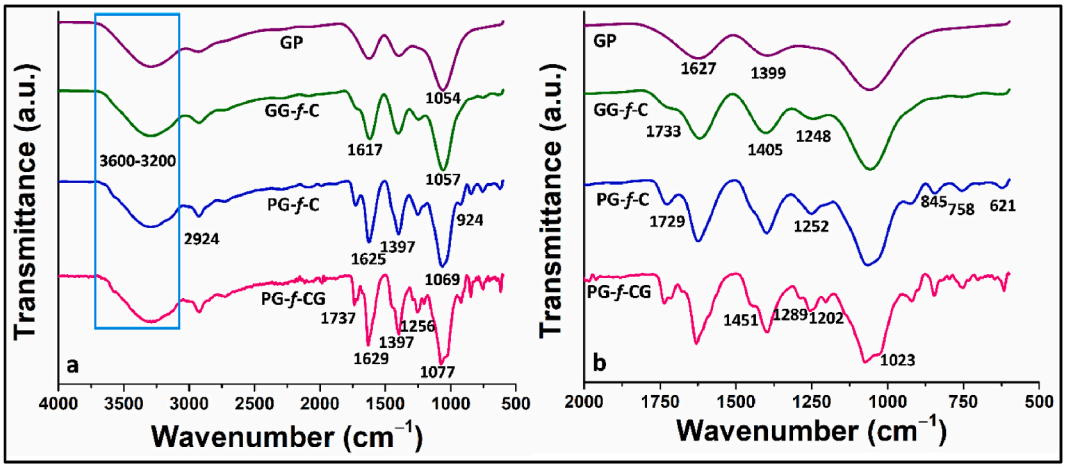

Fig. 2. The FTIR spectrum to determine the structural and functional group analysis. (a) FTIR spectrum ranging from 4000 to 500 cm^{-1} and (b) FTIR spectrum ranging from 2000 to 500 cm^{-1} of the fabricated hydrogels.

3.3. Statistical analysis

The data were presented as mean ± standard error, and the statistical data was analyzed using statistical software (IBM, SPSS Statistics 21). The mean ± S.E were calculated and presented as Y-error bars in the graphs. These error bars show standard deviations ($p < 0.05$; size of sample $n = 3$). $p < 0.001$ and optical density was $p < 0.05$.

4. Results and discussions

4.1. Structural analysis

The FTIR spectral profile of hydrogel films illustrates different vibration peaks corresponding to available functional groups, as shown in Fig. 2. The broadband 3600-3200 cm^{-1} was due to –OH functional groups available in GO, TEOS, PVA, gelatin, and CMC, confirming the intra/inter hydrogen bonding [30,31]. The peak positions at 1157 and 1064 cm^{-1} are because of stretching vibration C–O and O–H and attributed to the pyranose and confirm the effective crosslinking of gelatin, PVA, and CMC throughout the spectral profile via TEOS as crosslinker. A peak shifting was observed from 1057 to 1077 cm^{-1} that may be attributed to different interactions of polymeric chains (PVA, gelatin, and GO-*f*-CMC) in the presence of a crosslinker. The vibration peak at 2924 cm^{-1} corresponds to stretching vibration –CH, with a different intensity. An increase in the intensity of the broadband was found in GPs compared to PG-*f*-CGs. An asymmetric stretching vibration was observed at 1110 and 1000 cm^{-1}, and it was attributed to –Si–O–C and –Si–O–Si due to TEOS crosslink and confirmed the successful crosslinking among the polymeric chains [32]. The vibration peaks at 1737 and 1629 cm^{-1} are due to –C═C and –C═O stretching vibrations, respectively, and these are due to the graphene oxide, and increased intensity was observed from GG-*f*-C to PG-*f*-CG [33]. Henceforth, all the vibrational peaks corresponded with their positions and confirmed successful crosslinking for resultant fabricated hydrogels.

4.2. Surface morphological

The surface morphology of the fabricated freeze-dried has been determined at different magnifications (50–100 μm), as shown in Fig. 3(a–h). The surface morphology of the hydrogel at 100 μm provides a highly wrinkled and porous surface morphology (Fig. 3 (a–d)). In comparison, the porous surface morphology was found at 50 μm (Fig. 3(a–d)). These fabricated hydrogels exhibit unique surface morphologies from each other due to different chemical compositions. The surface morphology of these hydrogel films is different, and hydrogel formulations containing GO in their compositions have small islands. Hydrogel formulations without GO (i.e., PVA and gelatin crosslinked hydrogel (GP)) have flat or smooth surface morphology. The GO-incorporated hydrogels have highly uneven and rough morphology at different magnifications (100, and 50 μm), and the small clustering or island behavior of the GO was due to oven-drying. The slow water evaporation during oven drying caused the GO-sheet to be out, and these GO-sheets get close interactions due to interaction forces due to excessive functional groups of GO [34]. This GO-clustering may be micro/macro sized and provide rough surface morphology. It would be efficient for cell adherence, promoting cell proliferation and quick wound healing [35]. It can be seen that the regulated porosity with proper pore distribution was found, as shown in Fig. 3 (i-m to l-p). The porous material facilitates the exchange of gases, waste materials, and the supply of nutrients that promote cell viability and proliferation, which play an essential role in wound regeneration and repair. The highly irregular morphology may be necessary for other biomedical applications, including drug delivery, wound healing, and tissue engineering. The surface morphology of hydrogels plays a critical role in various wound healing applications, such as wound dressing [36,37]. The SEM micrographs have demonstrated that altering the

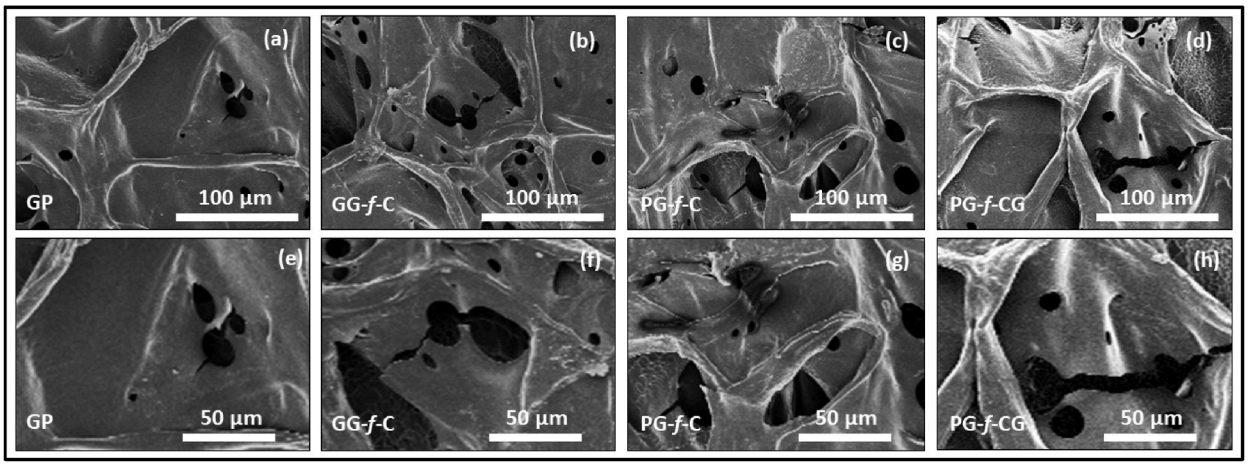

Fig. 3. The surface morphology of fabricated freeze-dried hydrogels was observed by SEM at different magnifications (a–d) 100 μm, and (e–h) 50 μm to evaluate surface behavior.

formulation of hydrogels can effectively produce hydrogels with distinct morphologies. Therefore, morphological analysis findings confirm that altering the composition of hydrogels can result in the fabrication of hydrogels with varying morphologies. It verifies that the synthesized hydrogels exhibit effective crosslinking and successful inclusion of graphene oxide.

4.3. Surface roughness

The surface topography can be measured by atomic force microscopy (AFM) as it provides information on the surface topography and roughness of hydrogels. We have performed the surface roughness analysis busing oven-dried hydrogel films as shown in Fig. 4 (e–l) and the surface roughness of the hydrogels has been presented in Fig. 4(a–d). All the hydrogels have different surface roughness, as shown in Fig. 4, which may be due to the different formulations of the hydrogel. Graphene oxide plays a vital role in surface roughness as hydrogel films incorporated with graphene oxide have more surface roughness than those without graphene oxide. A shift of surface roughness has been observed from GP to PG-*f*-CG (shown in Table 2), as GP has the least surface roughness and PG-*f*-CG has the maximum surface roughness, which could be the multifunctional behavior of the hydrogels. It also could be the reason that graphene oxide provides more active sites that cause more surface roughness, which is helpful for cell adherence and proliferation. Hence, incorporating graphene oxide into the multipolymeric hydrogel system would be an excellent material for wound healing applications due to increased cell viability and proliferation.

4.4. Physicochemical analysis

4.4.1. Wetting analysis

The wetting behavior of biomaterials is a vital surface phenomenon that determines the hydrophilic and hydrophobic behavior of the material. Additionally, it elucidates the interplay between biomaterial and biological processes during their interaction with biofluid [38]. The wetting characteristic can be adjusted to enhance cellular adhesion to the optimum surface of biomedical materials. The biomaterial possessing hydrophilic properties facilitates cellular processes that promote wound healing [39]. The wetting behavior of hydrogel was determined to evaluate the hydrophobicity and hydrophilicity at different time intervals (0 and 10 s), as shown in Fig. 5 (a). The oven-dried hydrogel samples were taken in this regard due to their smoother surface than the freeze-dried hydrogel samples. It was noticed that the hydrogels containing graphene oxide have a shifting trend from hydrophobicity to hydrophilicity. Also, all the hydrogel films exhibited an increased trend in hydrophilicity by increasing time from 0 to 10 s, as summarized in Table 3. It is worth mentioning that GO and polymeric chains (PVA, gelatin, and CMC) contain several –OH function groups that cause hydrophilicity due to the formation of hydrogen bonding [40]. It is also observed that hydrogels containing gelatin and CMC offered more swelling than PVA as biopolymers tend to absorb more water and make them a prominent material compared to synthetic polymers. The hydrophilicity trend in the hydrogel was found in the order PG-f-CG > GG-f-C > PG-f-C > PG. The maximum hydrophilic

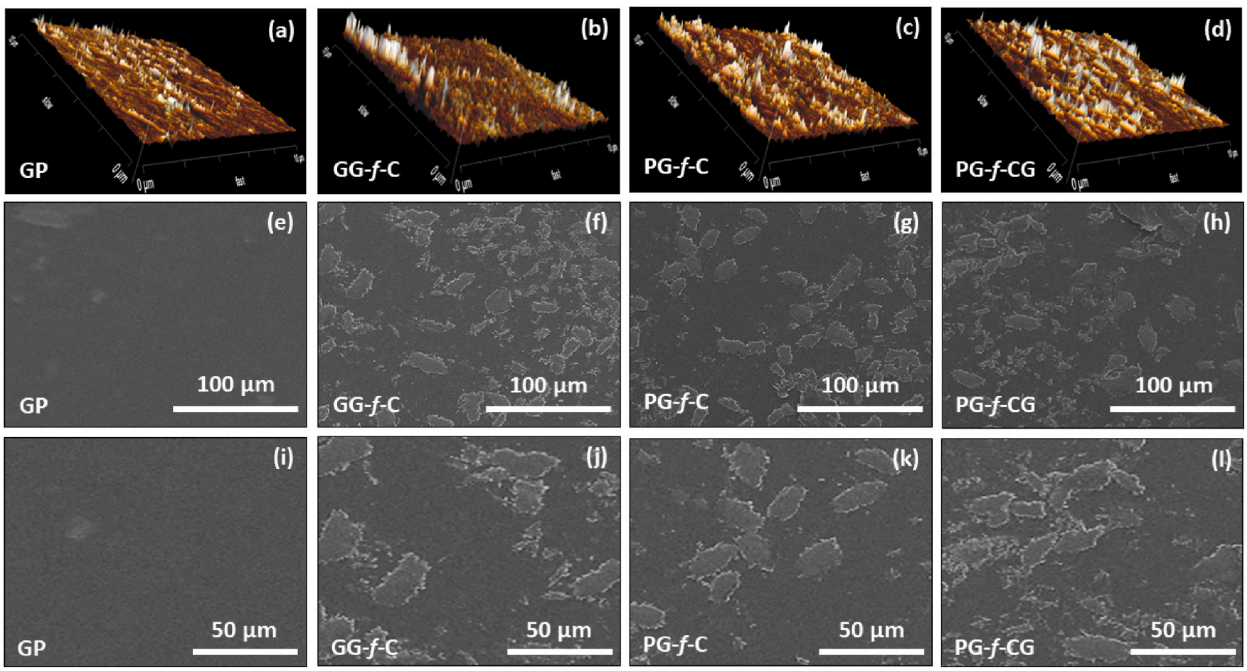

Fig. 4. The surface properties of the oven-dried hydrogels have been provided by surface roughness and surface morphology. (a–d) The surface roughness of the oven-dried hydrogels and surface morphology at different magnifications (100, and 50 µm) were performed to evaluate surface behavior.

Table 2
The surface roughness data of hydrogels has been summarized.

AFM parameters	GP	GG-*f*-C	PG-*f*-C	PG-*f*-CG
RMS (nm)	11.765	22.497	15.739	32.463
Skewness	0.237	0.378	0.216	0.439
Kurtosis	0.349	0.749	0.449	1.059
Surface area (μm^2)	14.486	29.184	21.793	35.496
Area percent (%)	0.913	7.267	3.497	11.891

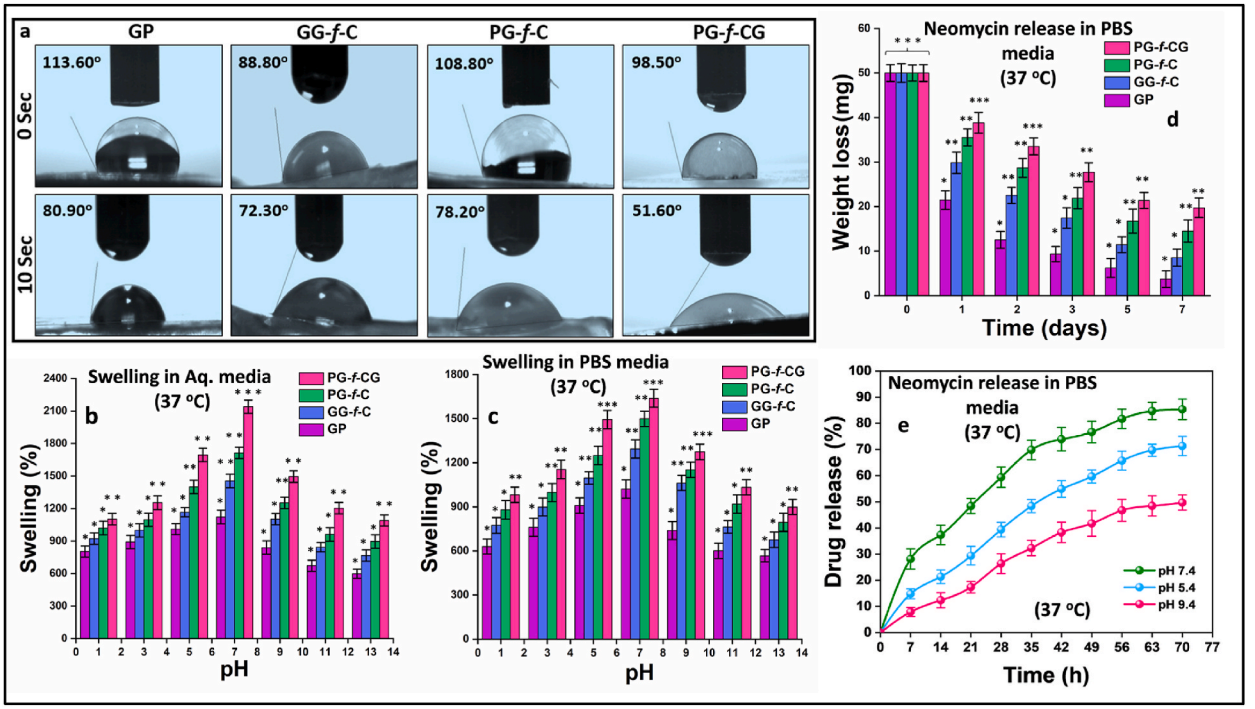

Fig. 5. The physicochemical behavior of the hydrogel samples was performed. (a) The wetting behavior was performed at room temperature at different intervals (0 and 10 Sec.) via a water contact system. (b and c) The swelling behavior of hydrogels in aqueous and PBS media at 37 °C, (d) degradation in PBS media at 37 °C, and a drug release assay was performed against hydrogel formulation (PG-*f*-CG) under different pH ranges (acidic, neutral, and basic) in PBS media at 37 °C.

Table 3
The physicochemical (wetting, swelling, and degradation) analyses were summarized.

Sample	Wetting (°)		Swelling (%)				Degradation (mg)	
			Aqueous Media		PBS Media			
	Max.	Min.	Max.	Min.	Max.	Min.	Max.	Min.
PG-*f*-CG	98.00	51.60	2139.73 ± 1.79	1089.51 ± 2.08	1639.17 ± 1.27	899.13 ± 1.05	38.82 ± 2.01	19.72 ± 2.25
PG-*f*-C	108.80	78.20	1454.83 ± 1.94	766.75 ± 1.90	1294.24 ± 1.34	676.81 ± 2.05	35.53 ± 2.94	14.49 ± 2.16
GG-*f*-C	88.80	72.30	1712.65 ± 1.63	895.19 ± 1.14	1499.92 ± 1.06	795.29 ± 2.84	29.84 ± 1.97	8.56 ± 2.47
GP	113.60	80.90	1121.49 ± 2.15	597.32 ± 0.84	1021.85 ± 1.89	567.01 ± 1.97	21.46 ± 1.25	3.72 ± 1.48

behavior of PG-*f*-CG is due to the incorporation of GO, gelatin, and CMC, as they contain several hydrophilic functional groups, which causes increased hydrogen bonding. Wettability may affect other physicochemical properties, such as swellability, surface charge, and degradation, which may affect biomedical properties [41,42]. These factors may also influence the cellular response to the biomaterial during and after implantation, potentially enhancing cell adherence and proliferation that promote wound healing.

4.4.2. Swelling analysis

The swelling of hydrogels was determined in aqueous and PBS media with different pH environments, at 37 °C. The objective was to assess the swelling of hydrogels in different pH media to determine their pH-stimuli response. Fig. 5 (b and c) presents the expansion of

the bioactive hydrogels in different media and reveals diverse responses dependent upon the pH levels of said medium. The hydrogels exhibited more significant swelling in aqueous environments with a pH of 7 (neutral pH) compared to acidic and basic conditions. The experimental findings revealed that the bioactive hydrogels exhibited more significant swelling in neutral pH than in acidic and basic pH. However, it was discovered that the hydrogels displayed a higher level of swelling in aqueous media than in PBS media. This observation suggests that the swelling characteristic of the hydrogels is more significant in aqueous environments compared to PBS media, as summarized in Table 2. In addition, it has been observed that hydrogels with graphene oxide exhibit a greater degree of swelling due to water molecules interacting with –OH functional groups. GO possesses multiple hydrophilic functional groups, such as –OH groups, which tend to interact with water due to increased hydrogen bonding to facilitate diffusion and perfusion. Excessive hydrogen bonding leads to more significant hydrogel swelling. It is also noticeable that hydrogels containing biopolymer chains and biopolymeric hydrogels offer more swelling properties due to their liquid absorption characteristics [43,44]. The notable swelling tendency of the material also facilitates the absorption of excessive wound exudate and blood resulting from spilled containers. Insufficient wound exudate can lead to bacterial colonization, perhaps leading to the development of chronic disease and subsequent limb amputation [45]. In addition, the substantial swelling of hydrogels at different pH levels could be crucial in the prolonged release of therapeutic chemicals encapsulated within the hydrogels. Consequently, the artificially produced bioactive hydrogels exhibit a notable ability to effectively absorb biofluids, rendering them promising biomaterials possessing desirable characteristics suitable for wound healing. Therefore, the observed variations in swelling behaviour of the composite hydrogels provide evidence of the effective crosslinking process.

4.4.3. Degradation analysis

The biodegradation analysis of the hydrogel was conducted in the phosphate buffer saline media at 37 °C with 7.4 pH, as shown in Fig. 5(d). The analysis confirms that all the hydrogel formulations incorporated with graphene oxide have a delayed degradation response compared to hydrogels lacking graphene oxide. It has been observed that all hydrogels have a similar degradation trend with different biodegradation behaviour. Among all the hydrogel samples, PG-*f*-CG hydrogel exhibited the lowest level of degradation, and GP hydrogel demonstrated the highest level, as summarized in Table 3. Specifically, it has been observed that hydrogel films incorporating graphene oxide exhibit a lower degradation rate, but hydrogel films containing gelatin and graphene oxide demonstrate a higher degradation rate than hydrogel films comprising polyvinyl alcohol and graphene oxide. The PG-*f*-CG has the lowest degradation rate due to its multipolymer composition, which imparts multifunctional capabilities and enhances its resistance to structural deterioration. It is noteworthy to add that the hydrogels with biopolymers exhibited a progressive degradation over an extended period. There are two main types of interaction in the polymeric matrix (covalent and H-bonding and other weaker van der Waals interactions) of the hydrogels, as illustrated in Fig. 1. These degradation mechanisms of hydrogel film could be either solubilization, breaking down the H-bonding and weak van der Waals forces of attraction, or degradation that may occur due to uncrosslinking and setting free polymeric chains [46,47]. During the wound healing process, the wound healing go through several phases, and the pH of the wound site may change. There is a possibility that the degradation may follow the mechanism of hydrolysis, which may fragment the long chains into small chains in a basic-pH media and cause the degradation [46,48]. The glycosidic interactions between its monomeric units may explain the biodegradation of carboxymethyl cellulose. In vivo, enzymatic actions can potentially break these fragile interactions in monomers. Small chain polysaccharides are dispersed due to enzymes' endurance in efficiently breaking down complicated polymeric structures [49,50]. Hence, the different crosslinking behaviour of the hydrogels exhibits that successful crosslinking exists between the polymeric chains of the composite hydrogels.

4.5. In vitro assay

4.5.1. Drug delivery assay

Achieving prolonged and regulated Neomycin release from the matrix of hydrogel polymers is a persistent challenge, primarily attributable to the intricate nature of its releasing process. Five primary characteristics govern drug release: diffusion, solvent, degradation, erosion, and swelling [51,52]. A hydrolytic process, in which the polymeric matrix of hydrogels starts to break down at its boundaries and periphery and releases the medication, facilitates drug delivery in the erosion pathway [53]. Drug release via a hydrogel polymer matrix occurs through diffusion processes driven by concentration differences. The diffusion mechanism and the phenomenon of hydrogel expansion are closely related. The interaction of hydrogels with physiological fluids facilitates it. Because the hydrogels can absorb biofluids, they will eventually expand volumetrically and release medication [54]. When the hydrogel is introduced to the trauma site, the dimensions of the polymeric mesh expand. Diffusion facilitates the swelling resulting from biofluid absorption, which is responsible for this rise. The hydrogels exhibit interactions with biofluids, leading to their dissolution and subsequent diffusion from the polymeric matrix of the hydrogel. The drug encapsulated within the polymeric matrix is subsequently released and made available at the surface of the matrix [55]. We have chosen the PG-*f*-CG hydrogel formulation for the controlled release of Neomycin due to its exceptional physicochemical characteristics. The optimal conditions for drug delivery are observed in a neutral environment with a pH of around 7.4 in phosphate-buffered saline (PBS) at a temperature of 37 °C. This phenomenon is observed despite all hydrogel samples being loaded with a model drug, Neomycin, which exhibits varied percentages of drug release. However, as depicted in Fig. 5(e)–a lower drug release was observed in acidic environments when considering the identical conditions. The minimum drug release was found in basic media from PG-*f*-CG, and it was observed that around 9 %, 16 %, and 28 % of drug release was observed from basic, acidic, and neutral pH-PBS media, respectively, after 7 h. Similarly, around 50 %, 73 %, and 87 % of drug releases were found in a similar order as above after 70 h. The drug release was observed at different pHs, and the fabricated hydrogel was pH-responsive and could release drugs under different pHs.

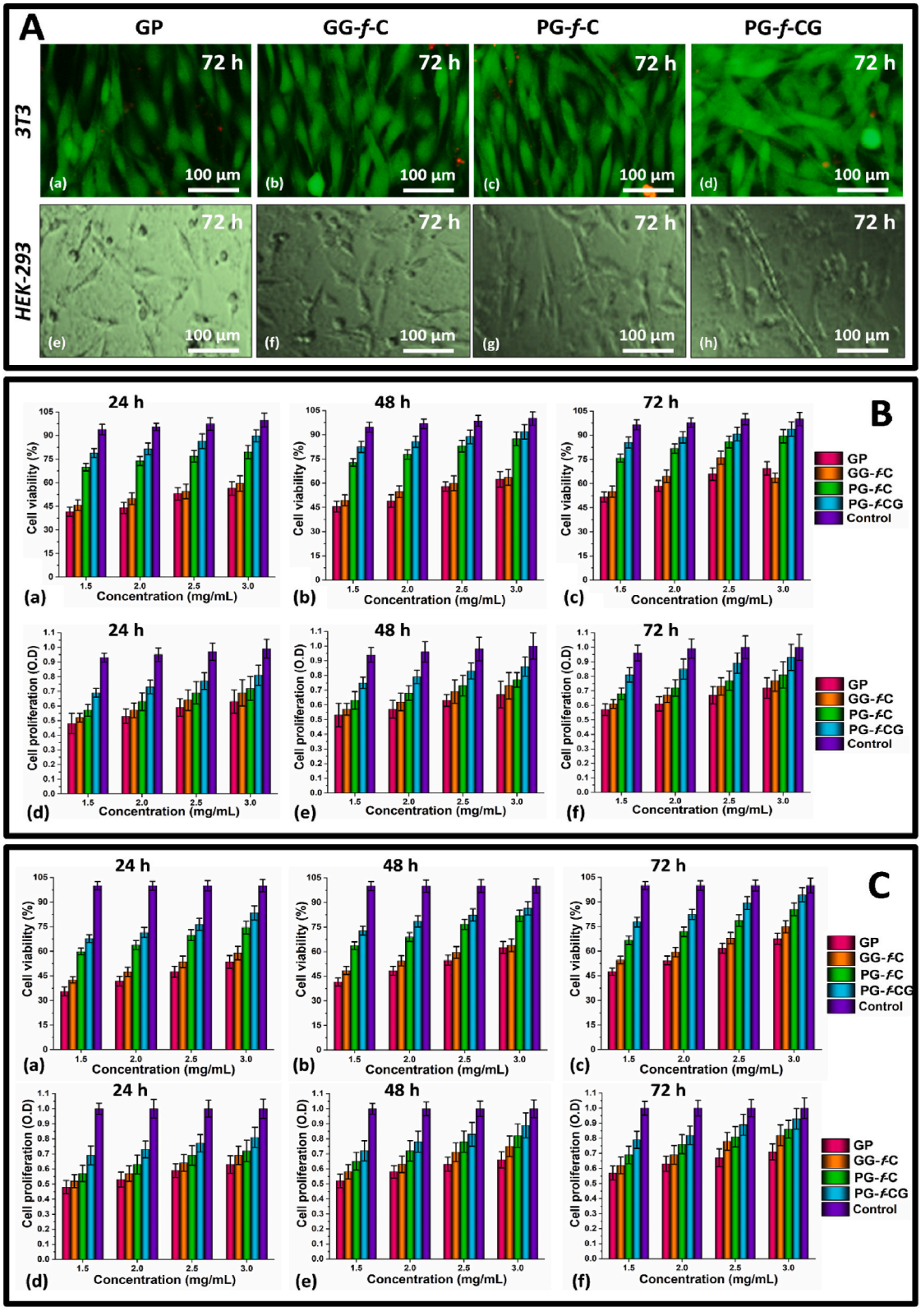

(caption on next page)

Fig. 6. The cellular behavior of the fabricated hydrogels against different cell lines (3T3 (a–d) and HEK-293 (e–f)). (A) The cell morphology after 72 h of all fabricated hydrogel formulations (a-). (B) Cell viability and proliferation of 3T3 cell lines (a–f) against all hydrogel formulations after different intervals (24, 48, and 72 h). (C) Cell viability and proliferation of HEK-293 cell lines (a–f) against all hydrogel formulations after different time intervals (24, 48, and 72 h).

4.5.2. Cell morphology

The cell morphology cells were performed against the hydrogels after 24, 48, and 72 h under standard in vitro settings. Studying the cellular behavior of the 3T3 and HEK-293 cell lines can provide valuable insights into the mechanisms behind wound healing processes when utilizing manufactured hydrogels as wound dressings for therapeutic applications [56]. The biological behavior of bioactive wound dressing material was performed using a range of biological studies to evaluate their biological potential for wound healing applications. Fig. 6(A) depicts the cellular morphology in response to several manufactured hydrogels after 72 h for 3T3. The cell population exhibited an increase in size and appropriate cylindrical shape as the contact duration was increased, as depicted in Fig. 6 (A). Additionally, minimal or no cell death was detected, as indicated by a red spot. The HEK-293 cell lines also have similar behavior cell morphological trends. Initially, they were found to be less populated, but after 72 h, they gained proper shape with the increasing cell population. Notably, the cells transitioning from GP to PG-*f*-CG exhibit developed cylinder-shaped and expanding shapes following 72 h. The change from GO to PG-*f*-CG resulted in the development of cell morphology; it could be due to the multifunctional and synergistic behavior of PG-*f*-CG due to multipolymer and graphene incorporation. The microenvironment provided by this particular entity exhibits considerable potential for facilitating cellular activities and promoting growth [57].

4.5.3. Cell viability and proliferation

Cell viability and proliferation assays were performed on 3T3 cell lines cultured on manufactured hydrogels at various concentrations and contact periods, as depicted in Fig. 6 (B–C). The cell viability and proliferation assays have found that the 3T3 and HEK-293 cell lines exhibit similar behavior. Since HEK-293 originated from the kidney and is a highly vascularized organ, these cell lines exhibit vascularization/angiogenesis. Specifically, it has been discovered that increased hydrogel contents and contact duration led to increased cell viability, as shown in Fig. 6B (a-c) and 6C (a-c). A similar trend of increasing cell proliferation was found in fabricated hydrogels against different concentrations, as shown in Fig. 6B (d-f) and 6C (d-f). The hydrogel sample PG-*f*-CG exhibited the maximum cell proliferation and viability, and GP offered the least in both cell lines. It may be due to the multifunctional behavior of PG-*f*-CG compared to GP. The fabricated hydrogel, potentially attributed to graphene oxide, gelatin, polyvinyl alcohol, and carboxymethyl cellulose, demonstrated the highest cell survival and proliferation levels. These entities provide favorable microenvironments due to their multifunctional and synergistic characteristics. The observed effects of these compounds involve the augmentation of cellular viability and proliferation via the provision of an additional active site and the interaction of functional groups through various weak intermolecular interactions, such as hydrogen bonding [58]. Therefore, the synthesized hydrogels have demonstrated remarkable cytocompatibility and vascularization/angiogenesis via cell viability and proliferation assays, suggesting their potential utility as dressings for soft tissue engineering and wound healing applications.

5. Conclusions

We have reported the fabricated multifunctional hydrogels from natural polymers (gelatin and carboxymethyl cellulose) and synthetic polymer (polyvinyl alcohol) by incorporating graphene oxide. It has been observed that the hydrogel PG-*f*-CG exhibits maximum hydrophilicity and superior open porous morphology that would be helpful for the exchange of gases (oxygen, carbon dioxide, and vapors), nutrient supply, and possible waste management than PG, GG-*f*-C, and PG-*f*-C. Because of its optimal properties for determining its drug release behavior under pH-responsive conditions, PG-f-CG has been chosen for the drug release study. It is because it exhibits essential swelling and degradation. It presents the sustained Neomycin in PBS media with different pH levels and confirms the stimulating drug release in a neutral pH environment. It was further observed that PG-*f*-CG exhibited excellent cytocompatibility and vascularization behavior with proper cell morphology due to its multifunctional behavior. Still, other in vitro and in vivo assays should be required to evaluate the excellent performance of the PG-*f*-CG is required. The fabricated hydrogels with controlled drug release would be promising for wound healing applications.

Ethical statement

This work was approved by the Ethics Committee of Shaanxi Provincial People's Hospital (No.2022K059).

Institutional review board statement

Not applicable.

Informed consent statement

Not applicable.

Data availability statement

All data to support the conclusions have been either provided or are otherwise publicly available.

CRediT authorship contribution statement

Liang Cheng: Writing – original draft, Methodology, Investigation. **Song Zhang:** Methodology, Investigation. **Qian Zhang:** Writing – original draft, Visualization, Resources. **Wenjie Gao:** Writing – review & editing, Resources, Methodology. **Benfeng Wang:** Writing – original draft, Visualization, Supervision. **Shengzhi Mu:** Writing – review & editing, Supervision.

Declaration of competing interest

All authors declared no conflict of interest.

Acknowledgement

This work was supported by the Natural Science Basic Research Program of Shaanxi (Grant No. 2023-JC-QN-0874) and the Industry-University-Research Innovation Fund of Science and Technology Development Center of the Ministry of Education (Grant No. 2021JH044).

References

[1] R. Sharma, A. Zamani, L.K. Dill, M. Sun, E. Chu, M.J. Robinson, T.J. O'Brien, S.R. Shultz, B.D. Semple, A systemic immune challenge to model hospital-acquired infections independently regulates immune responses after pediatric traumatic brain injury, J. Neuroinflammation 18 (2021) 1–23.
[2] M.U.A. Khan, M.A. Aslam, M.F.B. Abdullah, A. Hasan, S.A. Shah, G.M. Stojanović, Recent perspective of polymeric biomaterial in tissue engineering–a review, Mater. Today Chem. 34 (2023) 101818.
[3] K. Chen, H. Pan, D. Ji, Y. Li, H. Duan, W. Pan, Curcumin-loaded sandwich-like nanofibrous membrane prepared by electrospinning technology as wound dressing for accelerate wound healing, Mater. Sci. Eng. C 127 (2021) 112245.
[4] Y. Liang, J. He, B. Guo, Functional hydrogels as wound dressing to enhance wound healing, ACS Nano 15 (8) (2021) 12687–12722.
[5] A. Zhang, Y. Liu, D. Qin, M. Sun, T. Wang, X. Chen, Research status of self-healing hydrogel for wound management: a review, Int. J. Biol. Macromol. 164 (2020) 2108–2123.
[6] S. Jacob, A.B. Nair, J. Shah, N. Sreeharsha, S. Gupta, P. Shinu, Emerging role of hydrogels in drug delivery systems, tissue engineering and wound management, Pharmaceutics 13 (3) (2021) 357.
[7] Y. Zhong, H. Xiao, F. Seidi, Y. Jin, Natural polymer-based antimicrobial hydrogels without synthetic antibiotics as wound dressings, Biomacromolecules 21 (8) (2020) 2983–3006.
[8] X. Geng, Y. Qi, X. Liu, Y. Shi, H. Li, L. Zhao, A multifunctional antibacterial and self-healing hydrogel laden with bone marrow mesenchymal stem cell-derived exosomes for accelerating diabetic wound healing, Biomater. Adv. 133 (2022) 112613.
[9] F. Zarean, Z. Latifi, The effectiveness of self-healing (the healing codes) training on psychological capital and distress tolerance in women with addicted husbands, Curr. Psychol. (2020) 1–9.
[10] Q. Yu, S. Jin, S. Wang, H. Xiao, Y. Zhao, Injectable, adhesive, self-healing and conductive hydrogels based on MXene nanosheets for spinal cord injury repair, Chem. Eng. J. 452 (2023) 139252.
[11] D. Liu, J. Qiu, R. Xu, J. Liu, J. Feng, L. Ouyang, S. Qian, Y. Qiao, X. Liu, β-CD/PEI/PVA composite hydrogels with superior self-healing ability and antibacterial activity for wound healing, Compos. B Eng. 238 (2022) 109921.
[12] F. Li, S. Li, Y. Liu, Z. Zhang, Z. Li, Current advances in the roles of doped bioactive metal in biodegradable polymer composite scaffolds for bone repair: a mini review, Adv. Eng. Mater. 24 (8) (2022) 2101510.
[13] Y. Lu, M. Zhao, Y. Peng, S. He, X. Zhu, C. Hu, G. Xia, T. Zuo, X. Zhang, Y. Yun, A physicochemical double-cross-linked gelatin hydrogel with enhanced antibacterial and anti-inflammatory capabilities for improving wound healing, J. Nanobiotechnol. 20 (1) (2022) 1–26.
[14] N. Torabiardekani, F. Karami, M. Khorram, A. Zare, M. Kamkar, K. Zomorodian, Z. Zareshahrabadi, Encapsulation of Zataria multiflora essential oil in polyvinyl alcohol/chitosan/gelatin thermo-responsive hydrogel: synthesis, physico-chemical properties, and biological investigations, Int. J. Biol. Macromol. 243 (2023) 125073.
[15] S. Sreekumaran, A. Radhakrishnan, A.A. Rauf, G.M. Kurup, Nanohydroxyapatite incorporated photocrosslinked gelatin methacryloyl/poly (ethylene glycol) diacrylate hydrogel for bone tissue engineering, Progress in Biomaterials 10 (1) (2021) 43–51.
[16] M.U.A. Khan, S.I.A. Razak, A. Hassan, S. Qureshi, G.M. Stojanović, Multifunctional arabinoxylan-functionalized-graphene oxide based composite hydrogel for skin tissue engineering, Front. Bioeng. Biotechnol. 10 (2022) 865059.
[17] I. Behere, G. Ingavle, In vitro and in vivo advancement of multifunctional electrospun nanofiber scaffolds in wound healing applications: innovative nanofiber designs, stem cell approaches, and future perspectives, J. Biomed. Mater. Res. 110 (2) (2022) 443–461.
[18] M.U.A. Khan, G.M. Stojanović, R. Hassan, T.J.S. Anand, M. Al-Ejji, A. Hasan, Role of graphene oxide in bacterial Cellulose– gelatin hydrogels for wound dressing applications, ACS Omega 8 (18) (2023) 15909–15919.
[19] M.U. Aslam Khan, A. Haider, S.I. Abd Razak, M.R. Abdul Kadir, S. Haider, S.A. Shah, A. Hasan, R. Khan, S.u. d. Khan, I. Shakir, Arabinoxylan/graphene-oxide/nHAp-NPs/PVA bionano composite scaffolds for fractured bone healing, J. Tissue Eng. Regenerative Med. 15 (4) (2021) 322–335.
[20] W.S. Al-Arjan, M.U.A. Khan, H.H. Almutairi, S.M. Alharbi, S.I.A. Razak, pH-Responsive PVA/BC-f-GO dressing materials for burn and chronic wound healing with curcumin release kinetics, Polymers 14 (10) (2022) 1949.
[21] R. Khan, M.U. Aslam Khan, G.M. Stojanović, A. Javed, S. Haider, S.I. Abd Razak, Fabrication of bilayer nanofibrous-hydrogel scaffold from bacterial cellulose, PVA, and gelatin as advanced dressing for wound healing and soft tissue engineering, ACS Omega (2024).
[22] J. Wang, Q. Meng, Y. Ma, Y. Yang, R. Zhang, S. Zhong, J. Wang, Y. Gao, X. Cui, Enhanced carboxymethylcellulose-based hydrogels by curcumin-loaded microcapsules for promoting wound healing, ACS Sustain. Chem. Eng. 11 (51) (2023) 18074–18088.
[23] G. Chang, Q. Dang, C. Liu, X. Wang, H. Song, H. Gao, H. Sun, B. Zhang, D. Cha, Carboxymethyl chitosan and carboxymethyl cellulose based self-healing hydrogel for accelerating diabetic wound healing, Carbohydr. Polym. 292 (2022) 119687.
[24] Y. Yang, X. Zhao, J. Yu, X. Chen, R. Wang, M. Zhang, Q. Zhang, Y. Zhang, S. Wang, Y. Cheng, Bioactive skin-mimicking hydrogel band-aids for diabetic wound healing and infectious skin incision treatment, Bioact. Mater. 6 (11) (2021) 3962–3975.
[25] B.S. Alotaibi, M. Shoukat, M. Buabeid, A.K. Khan, G. Murtaza, Healing potential of neomycin-loaded electrospun nanofibers against burn wounds, J. Drug Deliv. Sci. Technol. 74 (2022) 103502.

[26] M. Ibrar, Y. Ayub, R. Nazir, M. Irshad, N. Hussain, Y. Saleem, M. Ahmad, Garlic and ginger essential oil-based neomycin nano-emulsions as effective and accelerated treatment for skin wounds' healing and inflammation: in-vivo and in-vitro studies, Saudi Pharmaceut. J. 30 (12) (2022) 1700–1709.
[27] J. Chen, D. Chen, J. Chen, T. Shen, T. Jin, B. Zeng, L. Li, C. Yang, Z. Mu, H. Deng, An all-in-one CO gas therapy-based hydrogel dressing with sustained insulin release, anti-oxidative stress, antibacterial, and anti-inflammatory capabilities for infected diabetic wounds, Acta Biomater. 146 (2022) 49–65.
[28] A. Ullah, A. Al Mamun, M.B. Zaidi, T. Roome, A. Hasan, A calcium peroxide incorporated oxygen releasing chitosan-PVA patch for Diabetic wound healing, Biomed. Pharmacother. 165 (2023) 115156.
[29] G. Repetto, A. Del Peso, J.L. Zurita, Neutral red uptake assay for the estimation of cell viability/cytotoxicity, Nat. Protoc. 3 (7) (2008) 1125–1131.
[30] S. Gilotra, D. Chouhan, N. Bhardwaj, S.K. Nandi, B.B. Mandal, Potential of silk sericin based nanofibrous mats for wound dressing applications, Mater. Sci. Eng. C 90 (2018) 420–432.
[31] M. Das, C. Sethy, C.N. Kundu, J. Tripathy, Synergetic reinforcing effect of graphene oxide and nanosilver on carboxymethyl cellulose/sodium alginate nanocomposite films: assessment of physicochemical and antibacterial properties, Int. J. Biol. Macromol. 239 (2023) 124185.
[32] A. Suhag, K. Biswas, S. Singh, A. Kulshreshtha, Crosslinking effect on polyvinyl alcohol resin for barrier properties of barrier biaxial orientation films, Prog. Org. Coating 163 (2022) 106662.
[33] C. Chen, G. Xiao, F. Zhong, S. Dong, Z. Yang, C. Chen, M. Wang, R. Zou, Silicon oxide encapsulated ZIF-8 loaded on reduced graphene oxide to improve flame retardancy of waterborne epoxy coatings, Prog. Org. Coating 163 (2022) 106605.
[34] M.U.A. Khan, G.M. Stojanović, R.A. Rehman, A.-R. Moradi, M. Rizwan, N. Ashammakhi, A. Hasan, Graphene oxide-functionalized bacterial cellulose–gelatin hydrogel with curcumin release and kinetics: in vitro biological evaluation, ACS Omega 8 (43) (2023) 40024–40035.
[35] G. Pan, F. Li, S. He, W. Li, Q. Wu, J. He, R. Ruan, Z. Xiao, J. Zhang, H. Yang, Mussel-and barnacle cement proteins-inspired dual-bionic bioadhesive with repeatable wet-tissue adhesion, multimodal self-healing, and antibacterial capability for nonpressing hemostasis and promoted wound healing, Adv. Funct. Mater. 32 (25) (2022) 2200908.
[36] H. Yu, X. Chen, J. Cai, D. Ye, Y. Wu, L. Fan, P. Liu, Novel porous three-dimensional nanofibrous scaffolds for accelerating wound healing, Chem. Eng. J. 369 (2019) 253–262.
[37] R. Khan, S. Haider, M.U.A. Khan, A. Haider, S.I. Abd Razak, A. Hasan, R. Khan, M.U. Wahit, Fabrication of amine-functionalized and multi-layered PAN-(TiO2)-gelatin nanofibrous wound dressing: in-vitro evaluation, Int. J. Biol. Macromol. 253 (2023) 127169.
[38] Z. Zhao, M. Pan, W. Yang, C. Huang, C. Qiao, H. Yang, J. Wang, X. Wang, J. Liu, H. Zeng, Bioinspired engineered proteins enable universal anchoring strategy for surface functionalization, J. Colloid Interface Sci. 650 (2023) 1525–1535.
[39] J.I. Kang, K.M. Park, Advances in gelatin-based hydrogels for wound management, J. Mater. Chem. B 9 (6) (2021) 1503–1520.
[40] M.U.A. Khan, S.I. Abd Razak, S. Haider, H.A. Mannan, J. Hussain, A. Hasan, Sodium alginate-f-GO composite hydrogels for tissue regeneration and antitumor applications, Int. J. Biol. Macromol. 208 (2022) 475–485.
[41] A. Ładniak, M. Jurak, A.E. Wiącek, Physicochemical characteristics of chitosan-TiO2 biomaterial. 2. Wettability and biocompatibility, Colloids Surf. A Physicochem. Eng. Asp. 630 (2021) 127546.
[42] M. Dziadek, K. Dziadek, K. Checinska, S. Salagierski, E. Choinska, P. Szatkowski, A. Wajda, A. Kopec, K. Cholewa-Kowalska, Polyphenolic compounds affect the long-term degradation behaviour of polymer and composite materials based on PCL, PLGA, and bioactive glass, Sustain. Mater. Technol. 35 (2023) e00568.
[43] N. Cohen, C.D. Eisenbach, A microscopically motivated model for the swelling-induced drastic softening of hydrogen-bond dominated biopolymer networks, Acta Biomater. 96 (2019) 303–309.
[44] M.U.A. Khan, G.M. Stojanovic, R. Hassan, T.J.S. Anand, M. Al-Ejji, A. Hasan, Role of graphene oxide in bacterial cellulose– gelatin hydrogels for wound dressing applications, ACS Omega 8 (18) (2023) 15909–15919.
[45] C. Qian, T. Zhang, J. Gravesande, C. Baysah, X. Song, J. Xing, Injectable and self-healing polysaccharide-based hydrogel for pH-responsive drug release, Int. J. Biol. Macromol. 123 (2019) 140–148.
[46] Y. Zhou, L. Jin, Hydrolysis-induced large swelling of polyacrylamide hydrogels, Soft Matter 16 (24) (2020) 5740–5749.
[47] M.U.A. Khan, I. Iqbal, M.N.M. Ansari, S.I.A. Razak, M.A. Raza, A. Sajjad, F. Jabeen, M. Riduan Mohamad, N. Jusoh, Development of antibacterial, degradable and ph-responsive chitosan/guar gum/polyvinyl alcohol blended hydrogels for wound dressing, Molecules 26 (19) (2021) 5937.
[48] M.U.A. Khan, G.M. Stojanović, M.F.B. Abdullah, A. Dolatshahi-Pirouz, H.E. Marei, N. Ashammakhi, A. Hasan, Fundamental properties of smart hydrogels for tissue engineering applications: a review, Int. J. Biol. Macromol. (2023) 127882.
[49] W. Li, Y. Bei, X. Pan, J. Zhu, Z. Zhang, T. Zhang, J. Liu, D. Wu, M. Li, Y. Wu, Selenide-linked polydopamine-reinforced hybrid hydrogels with on-demand degradation and light-triggered nanozyme release for diabetic wound healing, Biomater. Res. 27 (1) (2023) 49.
[50] S. Nazir, M.U.A. Khan, W.S. Al-Arjan, S.I. Abd Razak, A. Javed, M.R.A. Kadir, Nanocomposite hydrogels for melanoma skin cancer care and treatment: in-vitro drug delivery, drug release kinetics and anti-cancer activities, Arab. J. Chem. 14 (5) (2021) 103120.
[51] B. Liu, H. Zhu, D. Zhao, G. Nian, S. Qu, W. Yang, Hydrogel coating enabling mechanically friendly, step-index, functionalized optical fiber, Adv. Opt. Mater. 9 (20) (2021) 2101036.
[52] N. Zeng, L. He, L. Jiang, S. Shan, H. Su, Synthesis of magnetic/pH dual responsive dextran hydrogels as stimuli-sensitive drug carriers, Carbohydr. Res. 520 (2022) 108632.
[53] R. De Piano, D. Caccavo, S. Cascone, C. Festa, G. Lamberti, A.A. Barba, Drug release from hydrogel-based matrix systems partially coated: experiments and modeling, J. Drug Deliv. Sci. Technol. 61 (2021) 102146.
[54] H.E. Emam, T.I. Shaheen, Design of a dual pH and temperature responsive hydrogel based on esterified cellulose nanocrystals for potential drug release, Carbohydr. Polym. 278 (2022) 118925.
[55] Y. Herdiana, N. Wathoni, S. Shamsuddin, M. Muchtaridi, Drug release study of the chitosan-based nanoparticles, Heliyon (2021) e08674.
[56] L.T. Somasekharan, R. Raju, S. Kumar, R. Geevarghese, R.P. Nair, N. Kasoju, A. Bhatt, Biofabrication of skin tissue constructs using alginate, gelatin and diethylaminoethyl cellulose bioink, Int. J. Biol. Macromol. 189 (2021) 398–409.
[57] Y. Luo, X. Wei, P. Huang, 3D bioprinting of hydrogel-based biomimetic microenvironments, J. Biomed. Mater. Res. B Appl. Biomater. 107 (5) (2019) 1695–1705.
[58] P. Erkoc, I. Uvak, M.A. Nazeer, S.R. Batool, Y.N. Odeh, O. Akdogan, S. Kizilel, 3D printing of cytocompatible gelatin-cellulose-alginate blend hydrogels, Macromol. Biosci. 20 (10) (2020) 2000106.